

Article

Application of Homogenization Method in Free Vibration of Multi-Material Auxetic Metamaterials

Kadir Gunaydin ^{1,*}, Orhan Gülcan ¹ and Aykut Tamer ²¹ Türkiye Technology Center, General Electric Aerospace, 34880 İstanbul, Turkey; orhan.gulcan@ge.com² Department of Mechanical Engineering, University of Bath, Bath BA2 7AY, UK; at2849@bath.ac.uk

* Correspondence: kadir.gunaydin@ge.com

Abstract: Different additive manufacturing modalities enable the production of multi-material components which can be used in a wide range of industrial applications. The prediction of the mechanical properties of these components via finite element modelling rather than through testing is critical in terms of cost and time. However, due to the higher computational time spent on the modelling of lattice structures, different methods have been investigated to accurately predict mechanical properties. For this purpose, this study proposes the use of a homogenization method in the two most common types of multi-material lattices: honeycomb and re-entrant auxetics. Modal analyses were performed, and the first six mode shapes were extracted from explicit and implicit models. The results were compared in terms of mode shapes and natural frequencies. The results showed that homogenization can be successfully applied to multi-material honeycomb and re-entrant auxetic lattices without compromising the accuracy. It was shown that the implicit models predict the natural frequencies with an error range of less than 6.5% when compared with the explicit models in all of the mode shapes for both honeycomb and re-entrant auxetic lattices. The Modal Assurance Criteria, which is an indication of the degree of similarity between the mode shapes of explicit and implicit models, was found to be higher than 0.996, indicating very high similarity.

Keywords: homogenization; metamaterial; multi-material vibration; honeycomb; re-entrant



Academic Editor: Kefu Liu

Received: 25 November 2024

Revised: 10 January 2025

Accepted: 11 January 2025

Published: 13 January 2025

Citation: Gunaydin, K.; Gülcan, O.; Tamer, A. Application of Homogenization Method in Free Vibration of Multi-Material Auxetic Metamaterials. *Vibration* **2025**, *8*, 2. <https://doi.org/10.3390/vibration8010002>

Copyright: © 2025 by the authors. Licensee MDPI, Basel, Switzerland. This article is an open access article distributed under the terms and conditions of the Creative Commons Attribution (CC BY) license (<https://creativecommons.org/licenses/by/4.0/>).

1. Introduction

Auxetics are unique structures and a type of metamaterial whose mechanical properties are rarely observed in other materials. They exhibit a negative Poisson's ratio, meaning that in cases of compressive loading, they contract in both the direction of the applied load and the transverse direction, and similarly in cases of tension loading, the situation is the same but with elongation instead of contraction [1]. Due to their unique characteristics, they find usage in biomedical applications [2], in energy-dissipating structures [3,4], in crashworthiness tubes used in automotive and aerospace applications to increase energy absorption capability without considerably increasing the total weight [5–7], and in blast loading applications [8].

The mechanical properties of auxetic structures have been investigated in different scientific studies. Zhou et al. compared the additively manufactured hexagonal structure and two types of auxetic structures (double arrowhead and re-entrant). Their results revealed that the double arrowhead structure showed higher specific energy absorption and compressive strength than the other cellular structures [9]. Similar conclusions were also previously found by the authors [10]. Günaydin et al.'s study revealed that the re-entrant structure has lower energy absorption capability under quasi-static compression

than the anti-tetrachiral structure [11]. Aktas et al.'s study revealed that re-entrant auxetic structures have higher specific energy absorption than tetra-chiral auxetic structures [12]. Lu et al.'s study showed that the anti-tetrachiral auxetic structure has a higher energy absorption capability than hexachiral structures, and hierarchical design can be used to improve energy absorption ability [13]. Simpson and Kazanci's experimental studies revealed that crash boxes filled with re-entrant auxetic structures have lower specific energy absorption than those filled with honeycomb structures [14]. Gülcan's experimental study revealed that anti-tetrachiral lattices show higher energy absorption, mean crush force, and crush force efficiency than re-entrant and honeycomb lattices [15].

Auxetic structures also have very unique vibration characteristics like band gaps and directional wave propagation characteristics [16]. Namazinia et al. investigated the free vibration characteristics of a sandwich plate with a re-entrant auxetic core in a hygrothermal environment and stated that increasing the auxetic core thickness increases the fundamental natural frequencies [17]. Thang et al. investigated the free vibration of barrel-shaped sandwich shells with re-entrant auxetic cores and stated that different vibration modes resulted in fundamental natural frequencies that are highly dependent on geometric parameters [18]. Liu et al. proposed a novel auxetic structure embedded with resonators and showed that local resonant band gaps can be generated at lower frequencies [19]. Shoaie et al. proposed an analytical solution based on the multiple-scale method of perturbation for the free and forced vibrations of multilayer annular plates consisting of two top and bottom isotropic layers and one auxetic re-entrant layer [20]. Tran et al. investigated the free vibration characteristics of a sandwich panel with a re-entrant auxetic core and stated that increasing the side wall angle of the auxetic structure decreases the vibration frequency of the plate [21]. Similar conclusions were also reached by Sarafraz et al. [22]. They also stated that increasing the thickness of the auxetic re-entrant core and the thickness-to-length ratio generally resulted in a reduction in the natural frequencies.

It is important to predict the mechanical properties of components with auxetic structures through testing. However, since these tests are expensive and time consuming, mechanical analysis plays a very important role in predicting the real mechanical properties of these components. On the other hand, since these structures are so complex, it is very difficult to perform a mechanical analysis based on conventional finite element methods due to the high computational time and cost [23]. Generally, homogenization methods and their associated multiscale algorithms describe global behavior by reducing governing equations with rapidly varying coefficients to equations with effective coefficients, which can not only save computing resources, but also guarantee calculation precision.

In the homogenization theory, which was first applied to periodic domains using two-scale asymptotic expansions [24–26], the stiffness matrix can be reformed according to the unit cell topology and may show orthotropicity [27]. In the scientific literature, homogenization methods have been applied to different cellular structures and good correlations between classical finite element models and homogenized models have been observed [28–31]. Dirrenberger et al. applied homogenization to three different types of auxetic structures—hexachiral, tetra-antichiral, and rotachiral—and calculated the elastic moduli [32]. Reis and Ganghoffer applied homogenization to re-entrant hexagonal, hexachiral, cross chiral, rafter, and re-entrant square lattices and found good agreement between the homogenized results and the finite element simulation results [33]. El Nady et al. applied mechanical and numerical homogenization to auxetic structures to predict elastic responses, accounting for large changes in the geometry [34]. Wang et al. applied the strain-based expansion homogenization method to re-entrant auxetic structures and calculated the Young's modulus and Poisson's ratio in two principal directions. They found good

agreement between the theoretical, simulation, and experimental results [35]. Biswas et al. applied homogenization to tetra-chiral auxetic structures and stated that homogenization accurately captures the rotation of the central ring and the stretching of the tangential ligaments [36]. Zhang et al. applied homogenization to bowtie-shaped auxetic structures to obtain the equivalent stiffness and then used it in free and forced vibration analysis [37].

Since some additive manufacturing technologies enable the manufacturing of components with multiple materials, it is important to predict the mechanical properties of these components with analysis and/or homogenization methods. It is clear from a literature survey that most of the existing studies focus on the application of the homogenization theory to different types of auxetic structures. However, to the best of the authors' knowledge, no study so far has focused on using the homogenization theory in multi-material auxetic structures. To fill this gap, the present study focused on the feasibility of using the homogenization method in multi-material honeycomb and re-entrant auxetic structures. Modal analyses were performed, and the implicit and explicit analysis results were compared in terms of the first six deformation modes.

2. Materials and Methods

2.1. Unit Cell

In the present study, honeycomb and auxetic re-entrant structures were used as test cases. The corresponding unit cells are shown in Figure 1. Siemens NX 12 software (Siemens AG, Munich, Germany) was used to generate the geometries. Due to the advancements in additive manufacturing technology, components can be produced with multiple materials. Fused deposition modelling (FDM) [38] and material jetting [39] are two types of additive manufacturing modalities that enable the production of multi-material components. Considering the limitations of FDM and material jetting technologies, the ligament thicknesses of both topologies were set at 1.1 mm. To allow back-to-back comparison, the thickness and inner length were the same for the two lattice topologies.

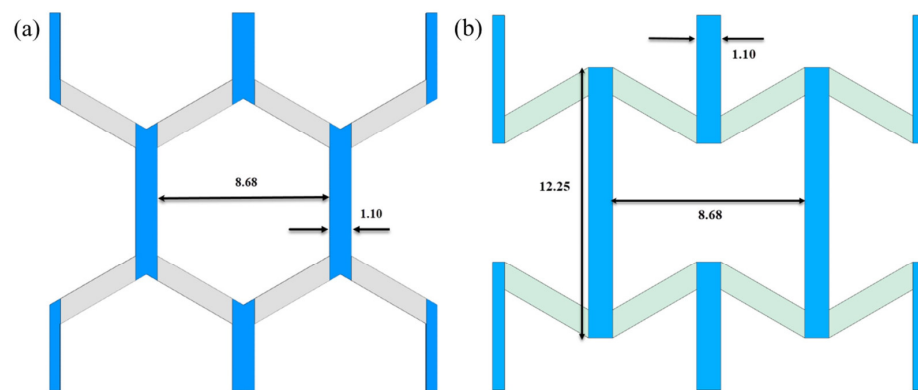


Figure 1. Unit cell topologies: (a) honeycomb, (b) re-entrant. Units are in mm.

2.2. Multi-Material Lattice Structure

The homogenization theory depends on a periodic arrangement of cell structures that are considerably smaller than the macroscopic scale. Ideally, these microscale units should be much smaller than the macroscopic scale. However, when optimizing to meet the minimum size constraints of existing additive manufacturing technologies, it is essential to identify the smallest cell size that effectively adheres to the principles of the homogenization theory [40]. In this paper, numerical studies are utilized to examine how the number of unit cells in a lattice structure affects the accuracy of homogenization. Figure 2 shows elastic modulus convergence in the z direction for honeycomb lattice topology. It is clear that after 5 unit cells, the elastic modulus in the z direction becomes almost constant. Since the

difference in elastic modulus in the z direction between 5 unit celled and 6 unit celled lattice structures is at an inconsiderable level, in the present study, 5 unit cells were stacked along the x and y directions to obtain the samples. In the present study, nylon and onyx (with chopped carbon fibers added to the nylon) were used as the input materials. Onyx was selected as a candidate material in the present study since it is a relatively new composite FDM material. As can be seen from Figure 3, onyx was selected as the material of the parallel ligaments (blue ligaments) and nylon was selected as that of other ligaments. The material properties of both materials are shown in Table 1.

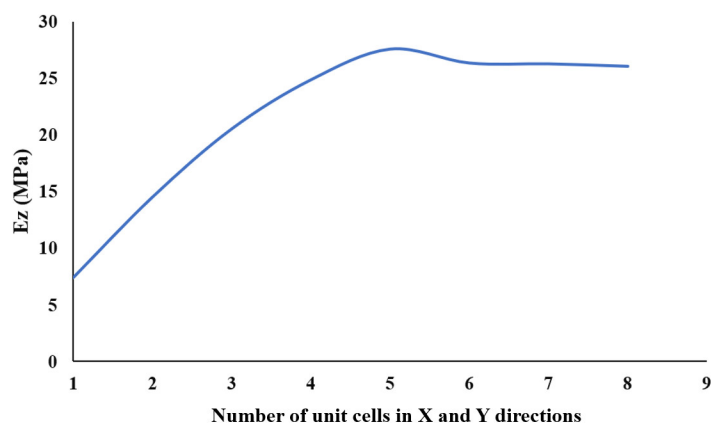


Figure 2. Elastic modulus convergence plot in z direction for honeycomb lattice structure.

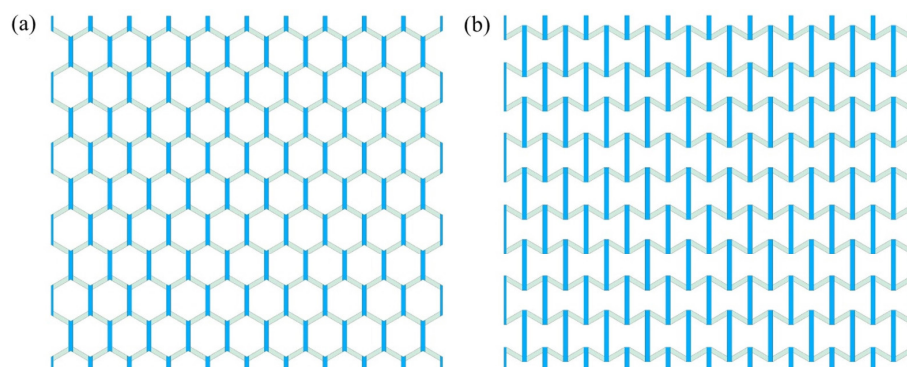


Figure 3. Test articles: (a) honeycomb, (b) re-entrant.

Table 1. Mechanical properties of nylon and onyx [41].

Material	Tensile Modulus (GPa)	Tensile Strength (MPa)	Density (g/cm ³)
Nylon	1.7	51	1.1
Onyx	2.4	40	1.2

2.3. Finite Element Model

Finite element models (FEM) were prepared using Ansys Workbench 2020, R2. Modal analyses were run both on the original geometries and the solid bodies that fit the outer boundaries of the original lattice structures. The free–free boundary condition that means that the lattice structure is free to move at its boundaries was used during analysis. The main advantage of using free boundaries is the elimination of the effects of boundary conditions. The natural frequencies and their related mode shapes were obtained from the modal analysis. The first six mode shapes were considered in the comparisons. Ansys Material Designer was used to obtain the equivalent material properties of the solid bodies. In Material Designer, anisotropic analyses were performed first, and it was observed that

the structures showed orthotropic behavior by considering the elastic modulus in different directions. Therefore, orthotropic analyses were used in Material Designer.

During homogenization, the effective elastic matrix of the honeycomb and auxetic re-entrant structures was estimated by applying strain loadings to the structures and solving the linear material constitutive relation via Hooke’s law ($\sigma = [C]\epsilon$). Due to the orthotropicity, 9 unknowns were used instead of 36 in the stiffness matrix (Equation (1)) [27]. Based on the stiffness matrix information extracted from Material Designer, unit cells of both the re-entrant and hexagonal lattice structures showed orthotropic elastic properties.

$$\begin{pmatrix} \sigma_{11} \\ \sigma_{22} \\ \sigma_{33} \\ \sigma_{12} \\ \sigma_{13} \\ \sigma_{23} \end{pmatrix} = \begin{bmatrix} C_{11} & C_{12} & C_{13} & C_{14} & C_{15} & C_{16} \\ C_{12} & C_{22} & C_{23} & C_{24} & C_{25} & C_{26} \\ C_{13} & C_{23} & C_{33} & C_{34} & C_{35} & C_{36} \\ C_{14} & C_{24} & C_{34} & C_{44} & C_{45} & C_{46} \\ C_{15} & C_{25} & C_{35} & C_{45} & C_{55} & C_{56} \\ C_{16} & C_{26} & C_{36} & C_{46} & C_{56} & C_{66} \end{bmatrix} \begin{pmatrix} \epsilon_{11} \\ \epsilon_{22} \\ \epsilon_{33} \\ \epsilon_{12} \\ \epsilon_{13} \\ \epsilon_{23} \end{pmatrix} \tag{1}$$

Since $C_{12} = C_{21}$, $C_{13} = C_{31}$, and $C_{23} = C_{32}$, due to symmetry, the stiffness matrix can be expressed as shown in Equation (2) [27].

$$\begin{pmatrix} \sigma_{11} \\ \sigma_{22} \\ \sigma_{33} \\ \sigma_{12} \\ \sigma_{13} \\ \sigma_{23} \end{pmatrix} = \begin{bmatrix} C_{11} & C_{12} & C_{13} & 0 & 0 & 0 \\ C_{12} & C_{22} & C_{23} & 0 & 0 & 0 \\ C_{31} & C_{32} & C_{33} & 0 & 0 & 0 \\ 0 & 0 & 0 & C_{44} & 0 & 0 \\ 0 & 0 & 0 & 0 & C_{55} & 0 \\ 0 & 0 & 0 & 0 & 0 & C_{66} \end{bmatrix} \begin{pmatrix} \epsilon_{11} \\ \epsilon_{22} \\ \epsilon_{33} \\ \epsilon_{12} \\ \epsilon_{13} \\ \epsilon_{23} \end{pmatrix} \tag{2}$$

$$C = \begin{bmatrix} 76.48 & 69.45 & 59.29 & 0.00 & 0.00 & 0.00 \\ 69.45 & 83.33 & 62.04 & 0.00 & 0.00 & 0.00 \\ 59.29 & 62.04 & 276.36 & 0.00 & 0.00 & 0.00 \\ 0.00 & 0.00 & 0.00 & 5.39 & 0.00 & 0.00 \\ 0.00 & 0.00 & 0.00 & 0.00 & 49.36 & 0.00 \\ 0.00 & 0.00 & 0.00 & 0.00 & 0.00 & 35.49 \end{bmatrix}$$

$$C = \begin{bmatrix} 71.65 & -51.26 & 11.26 & 0.00 & 0.00 & 0.00 \\ -51.26 & 59.07 & 0.08 & 0.00 & 0.00 & 0.00 \\ 11.26 & 0.08 & 321.07 & 0.00 & 0.00 & 0.00 \\ 0.00 & 0.00 & 0.00 & 1.31 & 0.00 & 0.00 \\ 0.00 & 0.00 & 0.00 & 0.00 & 35.23 & 0.00 \\ 0.00 & 0.00 & 0.00 & 0.00 & 0.00 & 39.24 \end{bmatrix}$$

After the homogenization of both the honeycomb and auxetic re-entrant structures, their stiffness matrices were obtained as seen above where the first one is result of homogenization of honeycomb structure and the second one is the result of the homogenization of auxetic re-entrant structure. As observed in stiffness matrix of re-entrant structure, negative elements exist, and this is caused by the unique characteristics of auxetic structures, which are related to their negative Poisson’s ratio.

2.4. Mesh Convergence

Quadrilateral elements were used in the discretization of the honeycomb and re-entrant structures due to the thin walls of their ligaments. Mesh size convergence studies were performed by conducting a series of simulations with different mesh sizes and considering the computational run time and accuracy by comparing the orthotropic material

properties that were obtained after the homogenization of the explicit unit cells of the lattice structures. The results showed that a mesh size of 0.2 mm is the convergence starting point; therefore, both lattices were discretized by using a mesh size of 0.2 mm. The related meshed geometries are shown in Figures 4 and 5, and the number of meshes and the number of nodes are shown in Table 2.

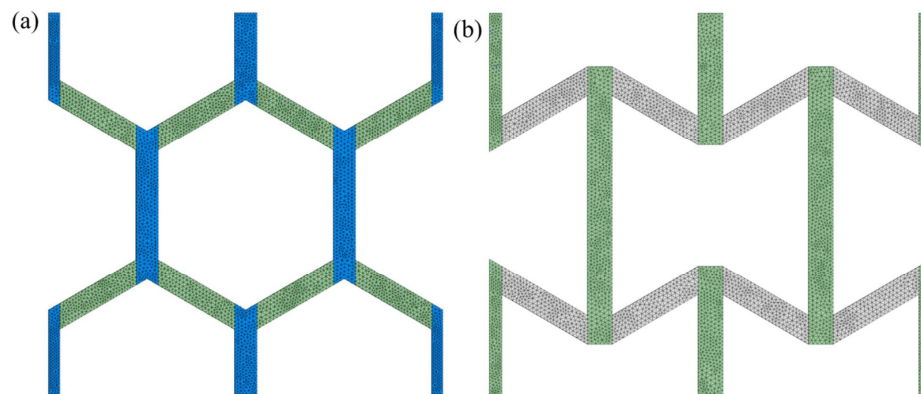


Figure 4. Meshed unit cells: (a) honeycomb, (b) re-entrant.

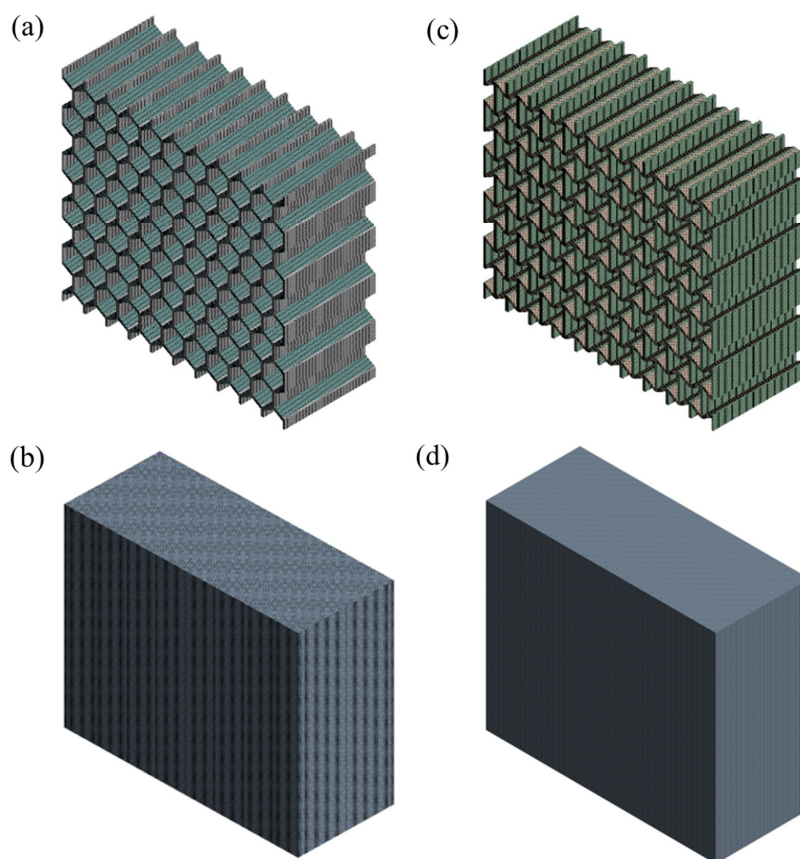


Figure 5. Meshed lattice structures: (a) honeycomb explicit, (b) honeycomb implicit, (c) re-entrant explicit, (d) re-entrant implicit.

In Figure 5, the explicit models are the macroscale models where discretization was applied to the full-scale geometry. On the other hand, the implicit models are homogenized models where, instead of modeling the entire macroscale, which requires greater computational resources, representative bulk volume was modelled. This representative bulk volume was generated based on the representative volume element, which is basically a single unit cell and can be patterned in different directions to obtain the final structure.

Homogenized or implicit models have equivalent material properties when compared with their explicit counterparts.

Table 2. Mesh type, number of nodes, and number of elements.

Model Type	Honeycomb		Re-entrant	
	Explicit	Implicit	Explicit	Implicit
Mesh type	Quadrilateral	Quadrilateral	Quadrilateral	Quadrilateral
Number of nodes	10,381,912	1,444,581	20,308,548	10,851,093
Number of elements	2,033,304	348,880	4,159,360	2,665,600

2.5. Mode Correlation

The Modal Assurance Criteria (MAC) [42] is a quantitative tool used in the field of structural dynamics to assess the similarity between mode shapes. The MAC is essentially a mathematical formula that compares the eigenvectors associated with these mode shapes. By comparing these eigenvectors, the MAC provides a numerical value between 0 and 1. This value serves as an indicator of the degree of similarity between the mode shapes of the different models or structures being compared. An MAC value close to 1 suggests a high degree of similarity, indicating that the mode shapes being compared are almost identical. Conversely, an MAC value near 0 implies little to no similarity, suggesting that the mode shapes are significantly different. By applying the MAC, it can be ensured that the natural frequencies and mode shapes of a structure are accurately identified, leading to more reliable and safe designs. The MAC can be expressed as follows:

$$\text{MAC} = \frac{|\phi_1^T \phi_2|^2}{(\phi_1^T \phi_1)(\phi_2^T \phi_2)} \quad (3)$$

where the matrices of the eigenvectors, ϕ_1 and ϕ_2 , are associated with two distinct sets of modal analyses. To determine the MAC value between two different geometries, including both implicit and explicit models, the MAC value was calculated for each pair of corresponding nodes that match within a 0.01 mm tolerance. However, due to the significant differences in the topology of the implicit and explicit geometries, the number of matching nodes is limited. Therefore, in this study, only the nodes that play a significant role in representing the modes were used to calculate the MAC values, and nodes at the edges of the geometries were selected.

3. Results and Discussion

As a result of the homogenization, the orthotropic material properties are calculated and presented in Table 3.

Table 3. Homogenized mechanical properties of re-entrant and honeycomb lattice structures (E, elastic modulus (GPa); G, shear modulus (GPa); ν , Poisson's ratio).

Material	E ₁	E ₂	E ₃	G ₁₂	G ₂₃	G ₁₃	ν_{12}	ν_{23}	ν_{13}
Re-entrant	0.027	0.022	0.316	0.001	0.035	0.039	0.868	0.025	0.035
Honeycomb	0.018	0.020	0.227	0.005	0.049	0.035	0.809	0.036	0.033

3.1. Honeycomb Structures

Total deformation with respect to the first six mode shapes for the honeycomb explicit and implicit models are shown in Table 4, and the natural frequencies of the honeycomb explicit and implicit models are tabulated in Table 5.

Table 4. First six mode shapes of honeycomb explicit and implicit models.

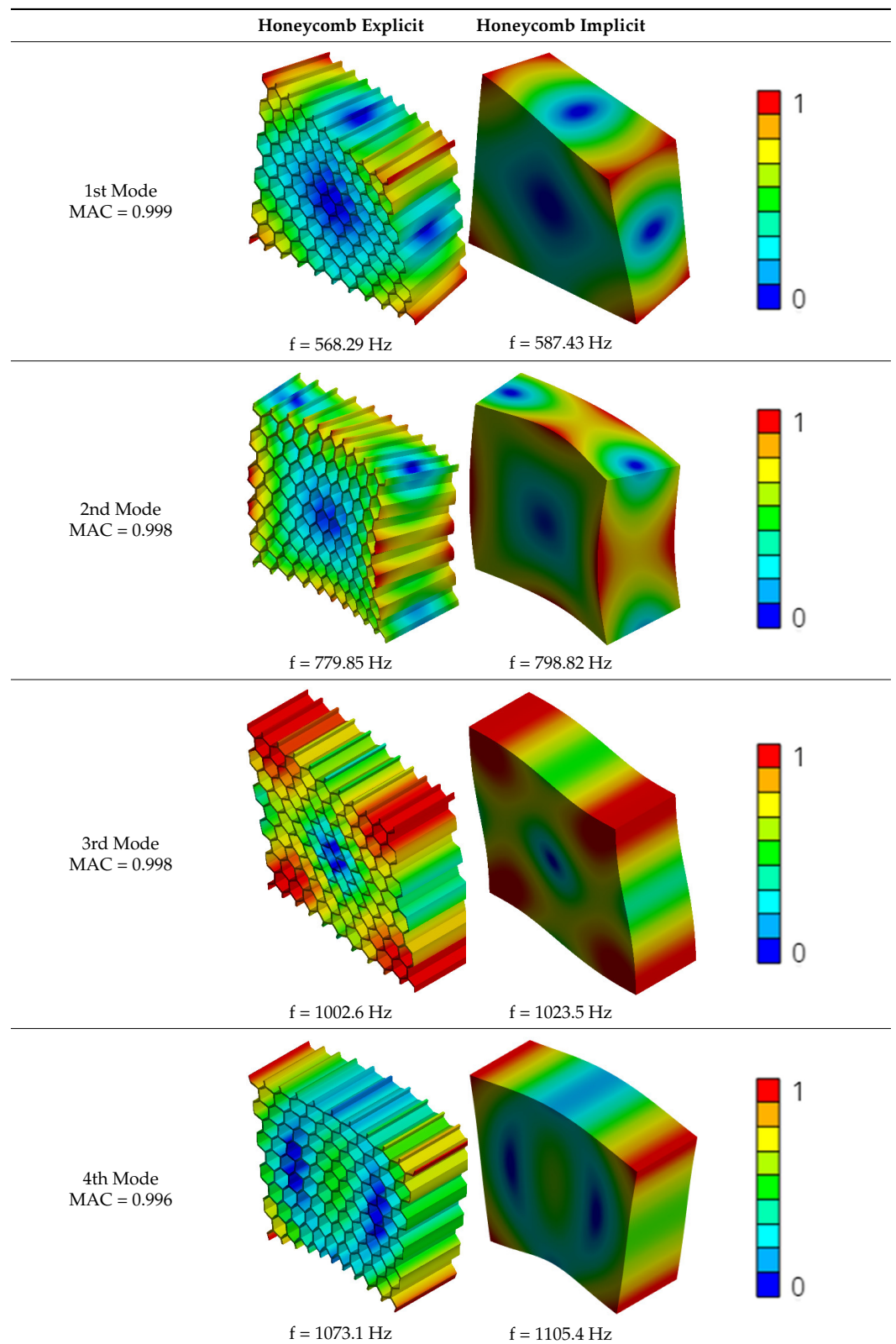


Table 4. *Cont.*

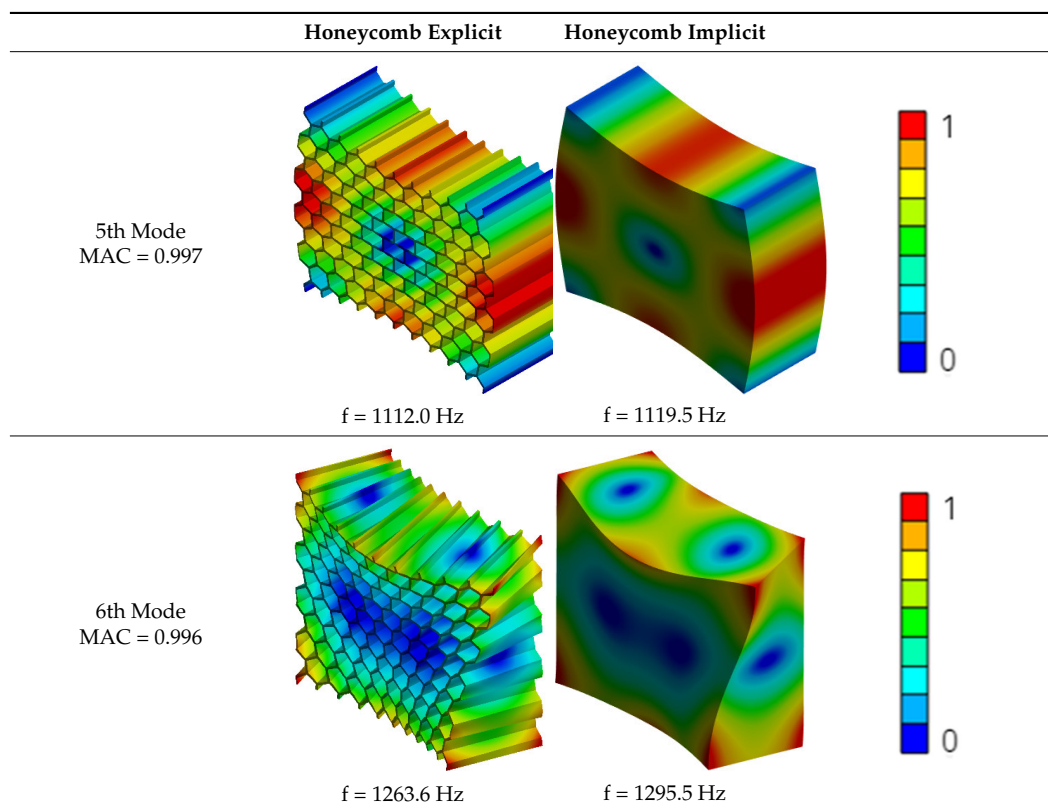


Table 5. Natural frequencies of honeycomb explicit and implicit models.

	Natural Frequencies (Hz)		
	Honeycomb Explicit	Honeycomb Implicit	Error (%)
First mode	568.29	587.43	3.4
Second mode	779.85	798.82	2.4
Third mode	1002.6	1023.5	2.1
Fourth mode	1073.1	1105.4	3.0
Fifth mode	1112.0	1119.5	0.7
Sixth mode	1263.6	1295.5	2.5

It is clear from Table 4 that there is a very good correlation between the implicit and explicit models for the first six mode shapes of the honeycomb lattice. Comparison of the natural frequencies based on the implicit and explicit models for the first six mode shapes (Table 5) reveals that a maximum error of 3.4% was found in the first mode. It is clear that the implicit models resulted in higher natural frequencies.

The MAC results of the honeycomb lattice structure are shown in Table 6. It is clear that a very good and satisfactory MAC correlation was found between the implicit and explicit models. Since the MAC number for the first six mode shapes is higher than 0.996, it can be stated that very high similarity is present between the natural frequencies found based on the implicit and explicit models.

Table 6. MAC results of honeycomb lattice structure.

		Implicit					
		587.4	798.8	1023.5	1105.4	1119.5	1295.5
Explicit	568.3	0.999	0	0	0	0	0
	779.9	0	0.998	0	0	0	0
	1002.6	0	0	0.998	0	0	0
	1073.1	0	0	0	0.996	0	0
	1121.0	0	0	0	0	0.997	0
	1263.6	0	0	0	0	0	0.996

3.2. Re-Entrant Structures

Total deformation with respect to the first six mode shapes for the re-entrant auxetic explicit and implicit models is shown in Table 7. Very good correlation can be observed between the six mode shapes based on the explicit and implicit models.

Table 7. First six mode shapes of re-entrant auxetic explicit and implicit models.

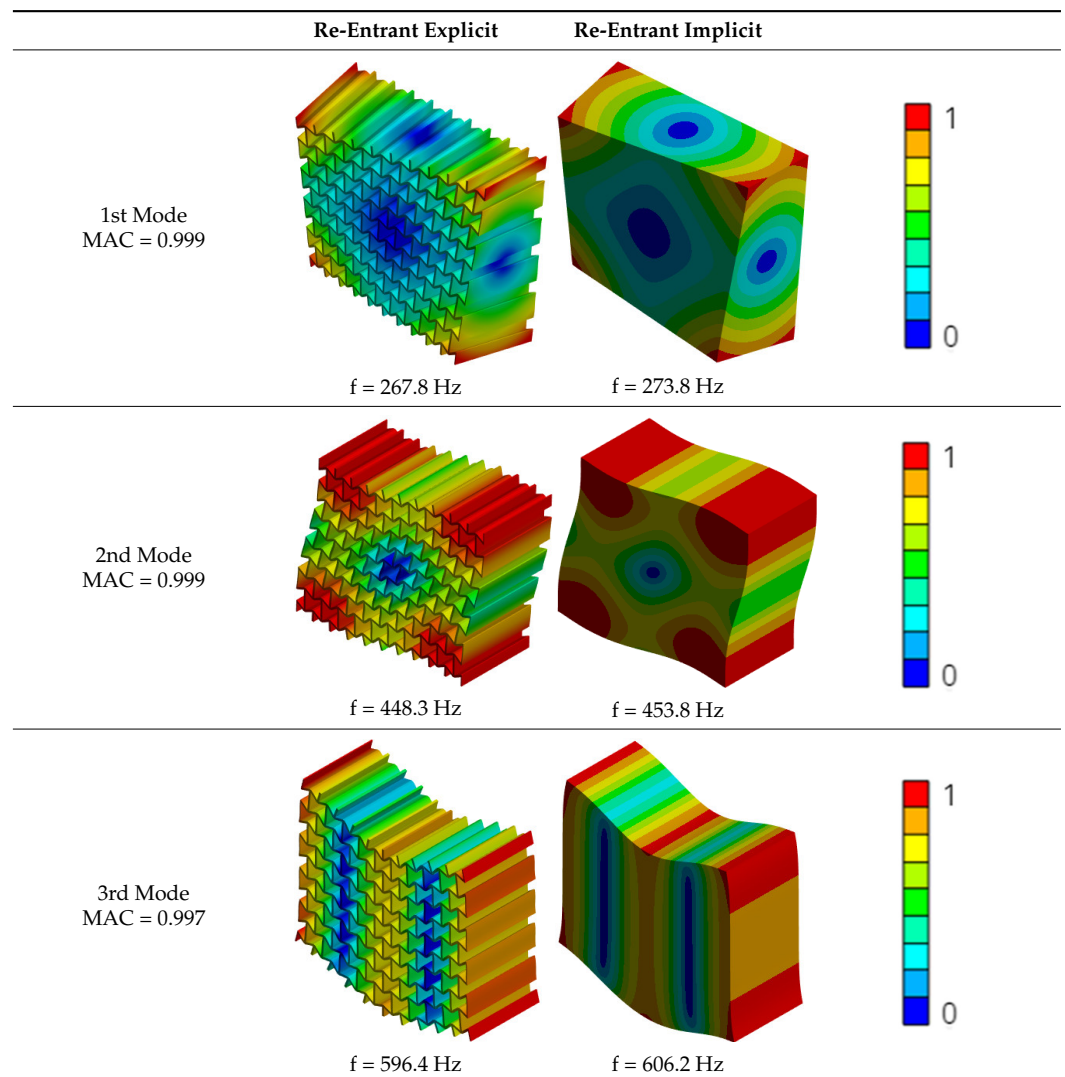


Table 7. Cont.

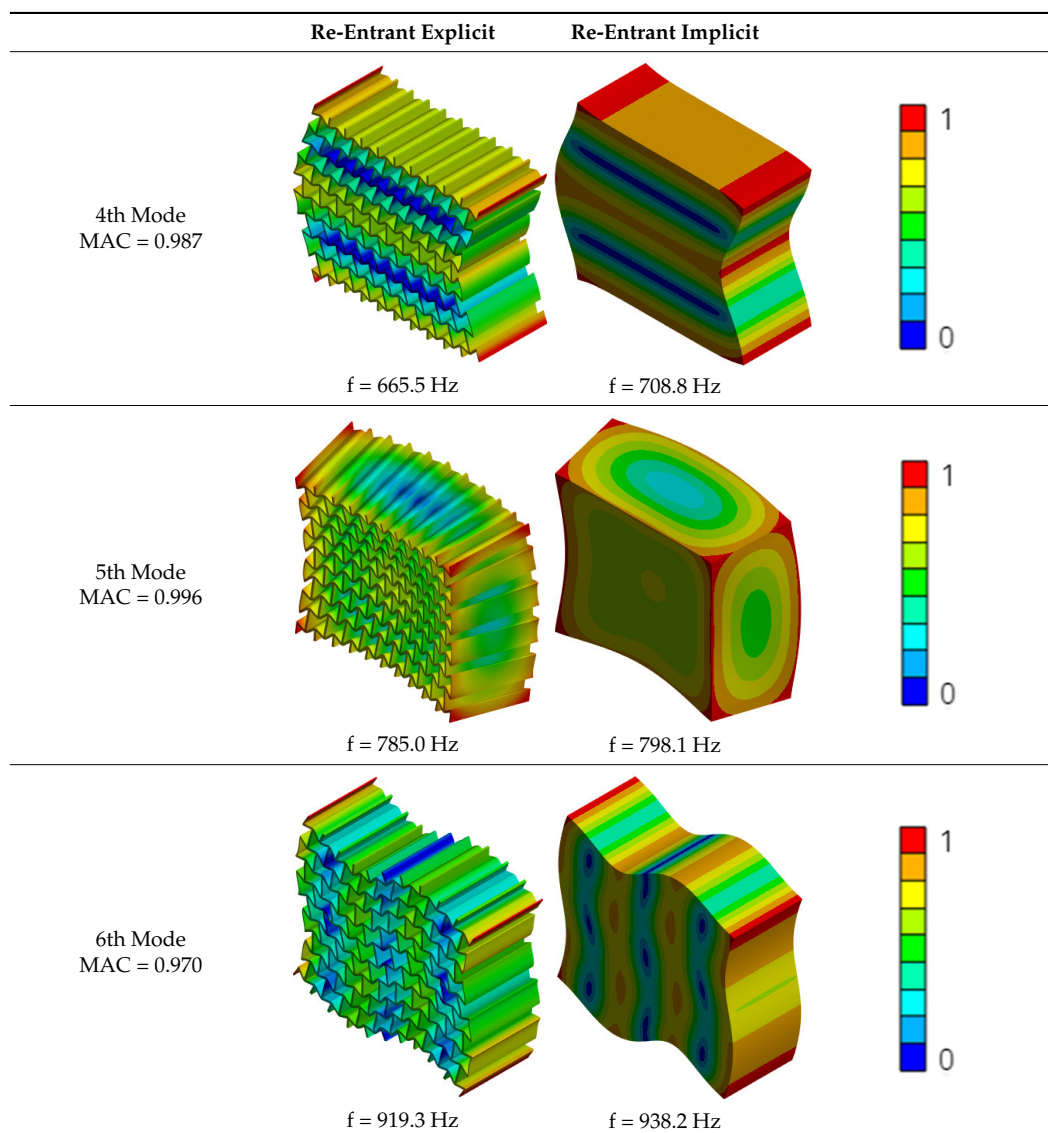


Table 8 shows the natural frequencies of the re-entrant auxetic explicit and implicit models for the first six mode shapes. The minimum and the maximum natural frequency errors between the explicit and implicit models were observed in the second (1.2%) and fourth mode (6.5%) shapes, respectively. It can be concluded that the implicit models accurately predict the natural frequencies within a 6.5% error range when compared to the explicit models. Similar to the honeycomb lattices, in the re-entrant auxetic lattices, the implicit models resulted in higher natural frequencies.

Table 8. Natural frequencies of re-entrant auxetic explicit and implicit models.

	Natural Frequencies (Hz)		
	Re-entrant Explicit	Re-entrant Implicit	Error (%)
First mode	267.8	273.8	2.2
Second mode	448.3	453.8	1.2
Third mode	596.4	606.2	1.6
Fourth mode	665.5	708.8	6.5
Fifth mode	785.0	798.1	1.7
Sixth mode	919.3	938.2	2.1

The MAC results of the re-entrant auxetic lattice structure are shown in Table 9. Similar to the honeycomb lattices, in the re-entrant auxetic lattices, a very good MAC correlation was found between the implicit and explicit models. The MAC number was found to be higher than 0.996 for the first six mode shapes.

Table 9. MAC results of re-entrant lattice structure.

		Implicit					
		273.8	453.8	606.2	708.8	798.1	938.2
Explicit	267.8	0.999	0	0	0	0	0
	448.3	0	0.999	0	0	0	0
	596.4	0	0	0.997	0	0	0
	665.5	0	0	0	0.987	0	0
	785.0	0	0	0	0	0.996	0
	919.3	0	0	0	0	0	0.970

4. Conclusions

This study investigated the efficiency of applying a homogenization method to two types of multi-material lattices: honeycomb and re-entrant auxetic. Modal analyses were performed, and the first six mode shapes were extracted from explicit and implicit models. The results were compared in terms of mode shape, maximum deformation, and natural frequency. The following main conclusions can be drawn:

- It was numerically shown that homogenization can be successfully used in the modal analysis of multi-material honeycomb and re-entrant auxetic lattices without compromising the accuracy. There is a good agreement between the explicit and implicit mode shapes for both lattices.
- Regarding the natural frequency, the error ranges between the implicit and explicit models are 0.7–3.4% for the honeycomb structure and 1.2–6.5% for the re-entrant auxetic structure.
- The MAC number was found to be higher than 0.996, which is an indication of very high similarities between the explicit and implicit models.

In this research, two elastic materials (nylon and onyx) were utilized. A further extension of this study may involve considering other complex material behaviors, such as viscoelasticity or anisotropy. Moreover, like the material, the manufacturing method changes the mechanical behavior of auxetic metamaterials, as stated in the literature [15]. Therefore, future studies may focus on the application of the homogenization method to different types of auxetic metamaterials produced by different manufacturing methods.

This study investigated the feasibility of the application of a homogenization method to multi-material auxetic metamaterials. Our future studies will focus on the experimental validation of the numerical results.

Moreover, comparisons with alternative state-of-the-art methodologies may be made to gain insight into the advantages and relative limitations of the proposed methodology [43,44].

Author Contributions: Conceptualization, K.G.; methodology, K.G.; software, K.G.; validation, K.G.; investigation, K.G., O.G. and A.T.; resources, K.G., O.G. and A.T.; data curation, K.G., O.G. and A.T.; writing—original draft preparation, O.G.; writing—review and editing, K.G., O.G. and

A.T.; visualization, K.G., O.G. and A.T. All authors have read and agreed to the published version of the manuscript.

Funding: This research received no external funding.

Data Availability Statement: The raw data supporting the conclusions of this article will be made available by the authors on request.

Conflicts of Interest: Authors Kadir Gunaydin and Orhan Gülcan were employed by the company General Electric Aerospace. The remaining authors declare that the research was conducted in the absence of any commercial or financial relationships that could be construed as a potential conflict of interest.

References

1. Hu, Q.; Zhang, X.; Zhang, J.; Lu, G.; Tse, K.M. A review on energy absorption performance of auxetic composites with fillings. *Thin-Walled Struct.* **2024**, *205*, 112348. [[CrossRef](#)]
2. Jiang, D.; Thissen, H.; Hughes, T.C.; Yang, K.; Wilson, R.; Murphy, A.B.; Nguyen, V. Advances in additive manufacturing of auxetic structures for biomedical applications. *Mater. Today Commun.* **2024**, *40*, 110045. [[CrossRef](#)]
3. Yin, H.; Zhang, W.; Zhu, L.; Meng, F.; Liu, J.; Wen, G. Review on lattice structures for energy absorption properties. *Compos. Struct.* **2023**, *304*, 116397. [[CrossRef](#)]
4. Wu, Y.; Fang, J.; Wu, C.; Li, C.; Sun, G.; Li, Q. Additively manufactured materials and structures: A state-of-the-art review on their mechanical characteristics and energy absorption. *Int. J. Mech. Sci.* **2023**, *246*, 108102.
5. Gomes, R.A.; de Oliveira, L.A.; Francisco, M.B.; Gomes, G.F. Tubular auxetic structures: A review. *Thin-Walled Struct.* **2023**, *188*, 110850. [[CrossRef](#)]
6. Hou, W.; He, P.; Yang, Y.; Sang, L. Crashworthiness optimization of crash box with 3D-printed lattice structures. *Int. J. Mech. Sci.* **2023**, *247*, 108198. [[CrossRef](#)]
7. Günaydin, K.; Gülcan, O.; Türkmen, H.S. Experimental and numerical crushing performance of crash boxes filled with re-entrant and anti-tetrachiral auxetic structures. *Int. J. Crashworthiness* **2023**, *28*, 649–663. [[CrossRef](#)]
8. Gülcan, O.; Günaydin, K.; Tamer, A. The effect of geometrical parameters on blast resistance of sandwich panels—A review. *Funct. Compos. Struct.* **2023**, *5*, 022001. [[CrossRef](#)]
9. Zhou, J.; Liu, H.; Dear, J.P.; Falzon, B.G.; Kazancı, Z. Comparison of different quasi-static loading conditions of additively manufactured composite hexagonal and auxetic cellular structures. *Int. J. Mech. Sci.* **2023**, *244*, 108054. [[CrossRef](#)]
10. Günaydin, K.; Gülcan, O. Air blast response of sandwich structures with auxetic cores under in-plane and axial loadings. *Res. Eng. Struct. Mater.* **2023**, *9*, 617–630. [[CrossRef](#)]
11. Günaydin, K.; Eren, Z.; Kazancı, Z.; Scarpa, F.; Grande, A.M.; Türkmen, H.S. In-plane compression behavior of anti-tetrachiral and re-entrant lattices. *Smart Mater. Struct.* **2019**, *28*, 115028. [[CrossRef](#)]
12. Aktas, C.; Acar, E.; Güler, M.A.; Altın, M. An investigation of the crashworthiness performance and optimization of tetra-chiral and reentrant crash boxes. *Mech. Based Des. Struct. Mach.* **2022**, *51*, 6881–6904. [[CrossRef](#)]
13. Lu, Q.; Qi, D.; Li, Y.; Xiao, D.; Wu, W. Impact energy absorption performances of ordinary and hierarchical chiral structures. *Thin-Walled Struct.* **2019**, *140*, 495–505.
14. Simpson, J.; Kazancı, Z. Crushing investigation of crash boxes filled with honeycomb and re-entrant (auxetic) lattices. *Thin-Walled Struct.* **2020**, *150*, 106676. [[CrossRef](#)]
15. Gülcan, O. Crashworthiness of laser powder bed fusion processed In718 auxetic metamaterials. *J. Braz. Soc. Mech. Sci. Eng.* **2024**, *46*, 414. [[CrossRef](#)]
16. Ji, J.C.; Luo, Q.; Ye, K. Vibration control based metamaterials and origami structures: A state-of-the-art review. *Mech. Syst. Signal Process.* **2021**, *161*, 107945.
17. Namazinia, N.; Alibeigloo, A.; Karimiasl, M. Free vibration and static analysis of sandwich composite plate with auxetic core and GPLRC facing sheets in hygrothermal environment. *Forces Mech.* **2024**, *15*, 100264. [[CrossRef](#)]
18. Thang, P.T.; Kim, H.; Kim, C.; Jang, H.; Kim, T.; Kim, J. Free vibration analysis of barrel-shaped sandwich shells with auxetic honeycomb core using modified thick shell theory. *Aerosp. Sci. Technol.* **2024**, *145*, 108861.
19. Liu, X.; Yang, J.; Li, S.; Fan, Y.; Yang, F.; Zhang, M.; Wu, L. Design, fabrication and vibration characteristics of a novel composite auxetic structure embedded with resonators. *Mater. Today Commun.* **2024**, *41*, 110420. [[CrossRef](#)]
20. Shoaie, A.G.; Eipakchi, H.; Nasrekani, F.M. Auxetic honeycomb core layer effect on vibrations of annular plates based on shear deformation theory. *Eng. Struct.* **2024**, *306*, 117855. [[CrossRef](#)]
21. Tran, H.; Vu, V.; Nguyen, V.; Tran, M. Free vibration and nonlinear dynamic response of sandwich plates with auxetic honeycomb core and piezoelectric face sheets. *Thin-Walled Struct.* **2023**, *191*, 111141. [[CrossRef](#)]

22. Sarafraz, M.; Seidi, H.; Kakavand, F.; Viliani, N.S. Free vibration and buckling analyses of a rectangular sandwich plate with an auxetic honeycomb core and laminated three-phase polymer/GNP/fiber face sheets. *Thin-Walled Struct.* **2023**, *183*, 110331. [[CrossRef](#)]
23. Mohandesi, N.; Talebitooti, M.; Fadaee, M. Mathematical modeling of free vibration of star-shaped auxetic rectangular plate. *Arch. Appl. Mech.* **2024**, *94*, 3455–3467. [[CrossRef](#)]
24. Babuška, I. Homogenization and its application. Mathematical and computational problems. In Proceedings of the Third Symposium on the Numerical Solution of Partial Differential Equations, College Park, MD, USA, 19–24 May 1976.
25. Bensoussan, A.; Lions, L.; Papanicolaou, G. Asymptotic analysis for periodic structures. In *Studies in Mathematics and Its Application*; North-Holland: Amsterdam, The Netherlands, 1978; Volume 5.
26. Sanchez-Palencia, E. Homogenization method for the study of composite media. In *Lecture Notes in Mathematics*; Verhulst, F., Ed.; Springer: Berlin/Heidelberg, Germany, 1983; Volume 985.
27. Blinowski, A.; Ostrowska-Maciejewska, J. On the elastic orthotropy. *Arch. Mech.* **1996**, *48*, 129–141.
28. Zhang, G.; Khandelwal, K. Computational design of finite strain auxetic metamaterials via topology optimization and nonlinear homogenization. *Comput. Methods Appl. Mech. Eng.* **2019**, *356*, 490–527. [[CrossRef](#)]
29. Mahapatra, B.P.; Sinha, V.; Maiti, D.K.; Jana, P. Active vibration suppression of tetrachiral auxetic core sandwich panel with CFRP skin: An RVE homogenization-assisted finite element approach. *Eur. J. Mech. A/Solids* **2024**, *106*, 105282. [[CrossRef](#)]
30. Ge, L.; Jiang, W.; Zhang, Y.; Tu, S.-T. Analytical evaluation of the homogenized elastic constants of plate-fin structures. *Int. J. Mech. Sci.* **2017**, *134*, 51–62. [[CrossRef](#)]
31. Ge, L.; Jiang, W.; Wang, Y.; Tu, S.-T. Creep-fatigue strength design of plate-fin heat exchanger by a homogeneous method. *Int. J. Mech. Sci.* **2018**, *146–147*, 221–233. [[CrossRef](#)]
32. Dirrenberger, J.; Forest, S.; Jeulin, D.; Colin, C. Homogenization of periodic auxetic materials. *Procedia Eng.* **2011**, *10*, 1847–1852. [[CrossRef](#)]
33. Reis, F.D.; Ganghoffer, J.F. Equivalent mechanical properties of auxetic lattices from discrete homogenization. *Comput. Mater. Sci.* **2012**, *51*, 314–321. [[CrossRef](#)]
34. El Nady, K.; Reis, F.D.; Ganghoffer, J.F. Computation of the homogenized nonlinear elastic response of 2D and 3D auxetic structures based on micropolar continuum models. *Compos. Struct.* **2017**, *170*, 271–290. [[CrossRef](#)]
35. Wang, T.; Wang, L.; Ma, Z.; Hulbert, G.M. Elastic analysis of auxetic cellular structure consisting of re-entrant hexagonal cells using a strain-based expansion homogenization method. *Mater. Des.* **2018**, *160*, 284–293. [[CrossRef](#)]
36. Biswas, R.; Poh, L.H.; Shedbale, A.S. A micromorphic computational homogenization framework for auxetic tetra-chiral structures. *J. Mech. Phys. Solids* **2020**, *135*, 103801. [[CrossRef](#)]
37. Zhang, M.; Zhong, Y.; Liu, X.; Liu, R. Applications of VAM-based homogenization model in free and forced vibrations of sandwich plates with bowtie-shaped auxetic core. *Compos. Struct.* **2023**, *314*, 116967. [[CrossRef](#)]
38. Günaydın, K.; Türkmen, H.S. Common FDM 3D printing defects. In Proceedings of the International Congress on 3D Printing (Additive Manufacturing) Technologies and Digital Industry, Antalya, Turkey, 19–21 April 2018.
39. Gülcan, O.; Günaydın, K.; Tamer, A. The state of the art of material jetting—A critical review. *Polymers* **2021**, *13*, 2829. [[CrossRef](#)] [[PubMed](#)]
40. Günaydın, K.; Yavuz, A.; Tamer, A. Free vibration characteristics of multi-material lattice structures. *Vibration* **2023**, *6*, 82–101. [[CrossRef](#)]
41. Li, D.; Dai, N.; Tang, Y.; Dong, G.; Zhao, Y.F. Design and optimization of graded cellular structures with triply periodic level surface-based topological shapes. *ASME J. Mech. Des.* **2019**, *141*, 071402. [[CrossRef](#)]
42. Pastor, M.; Binda, M.; Harčarik, T. Modal Assurance Criterion. *Procedia Eng.* **2012**, *48*, 543–548. [[CrossRef](#)]
43. Filippi, M.; Magliacano, D.; Petrolo, M.; Carrera, E. Variable-kinematics finite elements for propagation analyses of two-dimensional waveguides. In Proceedings of the 30th AIAA/CEAS Aeroacoustics Conference, Rome, Italy, 4–7 June 2024.
44. Filippi, M.; Magliacano, D.; Petrolo, M.; Carrera, E. Wave propagation in prestressed structures with geometric nonlinearities through carrera unified formulation. In Proceedings of the 30th AIAA/CEAS Aeroacoustics Conference, Rome, Italy, 4–7 June 2024.

Disclaimer/Publisher’s Note: The statements, opinions and data contained in all publications are solely those of the individual author(s) and contributor(s) and not of MDPI and/or the editor(s). MDPI and/or the editor(s) disclaim responsibility for any injury to people or property resulting from any ideas, methods, instructions or products referred to in the content.